Structures, photoluminescence and photocatalytic properties of two novel metal-organic frameworks based on tetrazole derivatives

Qi Zhang, [§] Dong Chen, [§] Xuan He,[*] Shiliang Huang, Jinglun Huang, Xiaoqing

Zhou,[*] Zongwei Yang, Jinshan Li, Hongzhen Li,[*] and Fude Nie

Institute of Chemical Materials, China Academy of Engineering Physics, Mianyang

621900, China.

[*]Address for correspondence. Email: xuan.hellen@gmail.com

Phone: 86-816-2493145; Fax: 86-816-2486342

[§]Author Contributions

Qi Zhang and Dong Chen contributed equally to this work.

Table 1. Bond lengths [Å] for **1**.

Ag(1)-N(4)#1	2.207(5)	N(1)-N(2)	1.351(8)
Ag(1)-N(1)	2.208(5)	N(2)-N(3)	1.299(7)
Ag(1)-N(2)#2	2.273(5)	N(2)-Ag(1)#2	2.273(5)
C(1)-N(4)	1.338(8)	N(3)-N(4)	1.354(6)
C(1)-N(1)	1.338(8)	N(4)-Ag(1)#3	2.207(5)
C(1)-N(5)	1.374(8)	N(5)-H(5A)	0.8800
		N(5)-H(5B)	0.8800

Symmetry transformations used to generate equivalent atoms:

#1 x+1,-y+3/2,z+1/2   #2 -x+1,-y+2,-z+2   #3 x-1,-y+3/2,z-1/2

Table 2. Bond angles [°] for **1**.

N(4)#1-Ag(1)-N(1)	134.16(19)	N(3)-N(2)-Ag(1)#2	126.1(4)
N(4)#1-Ag(1)-N(2)#2	113.79(19)	N(1)-N(2)-Ag(1)#2	122.5(4)
N(1)-Ag(1)-N(2)#2	112.0(2)	N(2)-N(3)-N(4)	108.9(5)
N(4)-C(1)-N(1)	111.0(6)	C(1)-N(4)-N(3)	105.2(5)
N(4)-C(1)-N(5)	125.4(6)	C(1)-N(4)-Ag(1)#3	130.6(4)
N(1)-C(1)-N(5)	123.4(6)	N(3)-N(4)-Ag(1)#3	122.9(4)
C(1)-N(1)-N(2)	104.6(5)	C(1)-N(5)-H(5A)	120
C(1)-N(1)-Ag(1)	132.2(5)	C(1)-N(5)-H(5B)	120
N(2)-N(1)-Ag(1)	122.6(4)	H(5A)-N(5)-H(5B)	120
N(3)-N(2)-N(1)	110.3(5)	N(3)-N(2)-Ag(1)#2	126.1(4)

Symmetry transformations used to generate equivalent atoms:

#1 x+1,-y+3/2,z+1/2   #2 -x+1,-y+2,-z+2   #3 x-1,-y+3/2,z-1/2

Table 3. Bond lengths [Å] for **2**.

Ag(1)-N(1)	2.244(2)	N(3)-C(1)	1.334(3)
Ag(1)-N(2)#1	2.250(2)	N(4)-N(5)	1.335(3)
Ag(1)-N(3)	2.385(2)	N(5)-N(6)	1.338(3)
Ag(1)-N(7)#2	2.572(2)	N(6)-C(1)	1.329(3)
N(1)-C(2)	1.481(4)	N(7)-N(7)#2	1.258(4)
N(1)-H(1N)	0.93(4)	N(7)-C(1)	1.403(3)
N(1)-H(2N)	0.90(4)	N(7)-Ag(1)#2	2.572(2)
N(2)-C(3)	1.464(4)	C(2)-C(3)	1.515(4)
N(2)-Ag(1)#3	2.250(2)	C(2)-H(2A)	0.99
N(2)-H(4N)	0.83(4)	C(2)-H(2B)	0.99
N(2)-H(3N)	0.95(5)	C(3)-H(3A)	0.99
N(3)-N(4)	1.333(3)	C(3)-H(3B)	0.99

Symmetry transformations used to generate equivalent atoms:

#1 -x+1,y-1/2,-z+1/2   #2 -x+1,-y+1,-z+1   #3 -x+1,y+1/2,-z+1/2

Table 4. Bond angles [°] for **2**.

N(1)-Ag(1)-N(2)#1	128.85(8)	N(3)-N(4)-N(5)	109.6(2)
N(1)-Ag(1)-N(3)	113.21(8)	N(4)-N(5)-N(6)	109.0(2)
N(2)#1-Ag(1)-N(3)	112.09(8)	C(1)-N(6)-N(5)	104.4(2)
N(1)-Ag(1)-N(7)#2	122.59(8)	N(7)#2-N(7)-C(1)	112.8(3)
N(2)#1-Ag(1)-N(7)#2	97.02(8)	N(7)#2-N(7)-Ag(1)#2	119.1(2)
N(3)-Ag(1)-N(7)#2	65.56(7)	C(1)-N(7)-Ag(1)#2	127.91(15)
C(2)-N(1)-Ag(1)	116.77(18)	N(6)-C(1)-N(3)	112.8(2)
C(2)-N(1)-H(1N)	106(3)	N(6)-C(1)-N(7)	120.7(2)
Ag(1)-N(1)-H(1N)	108(2)	N(3)-C(1)-N(7)	126.5(2)
C(2)-N(1)-H(2N)	109(2)	N(1)-C(2)-C(3)	111.7(2)
Ag(1)-N(1)-H(2N)	104(2)	N(1)-C(2)-H(2A)	109.3
H(1N)-N(1)-H(2N)	112(4)	C(3)-C(2)-H(2A)	109.3
C(3)-N(2)-Ag(1)#3	114.86(17)	N(1)-C(2)-H(2B)	109.3
C(3)-N(2)-H(4N)	108(3)	C(3)-C(2)-H(2B)	109.3
Ag(1)#3-N(2)-H(4N)	111(3)	H(2A)-C(2)-H(2B)	107.9
C(3)-N(2)-H(3N)	114(3)	N(2)-C(3)-C(2)	114.2(2)
Ag(1)#3-N(2)-H(3N)	111(3)	N(2)-C(3)-H(3A)	108.7
H(4N)-N(2)-H(3N)	96(4)	C(2)-C(3)-H(3A)	108.7
N(4)-N(3)-C(1)	104.1(2)	N(2)-C(3)-H(3B)	108.7
N(4)-N(3)-Ag(1)	139.92(18)	C(2)-C(3)-H(3B)	108.7
C(1)-N(3)-Ag(1)	115.89(17)	H(3A)-C(3)-H(3B)	107.6

Symmetry transformations used to generate equivalent atoms:

#1 -x+1,y-1/2,-z+1/2   #2 -x+1,-y+1,-z+1   #3 -x+1,y+1/2,-z+1/2

The band gap sizes of **1** and **2** were investigated by UV-vis diffuse reflection measurement method at room temperature. The $(Ah\nu)^2$ vs hν curves for products are shown in Figure S1 and S2. According to the equation $Ah\nu = (h\nu - Eg)^{n/2}$ (where A is the absorption, hν is the discrete photo energy, n is a constant, and Eg is the band gap energy), the extrapolated value (the straight lines to the x axis) of hν at A = 0 give absorption edge energies corresponding to Eg = 3.29 and 2.12 eV for **1** and **2**, respectively.[1, 2]

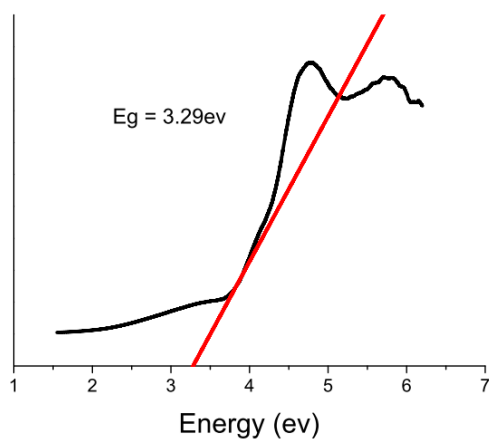Eg = 3.29ev

Energy (ev)

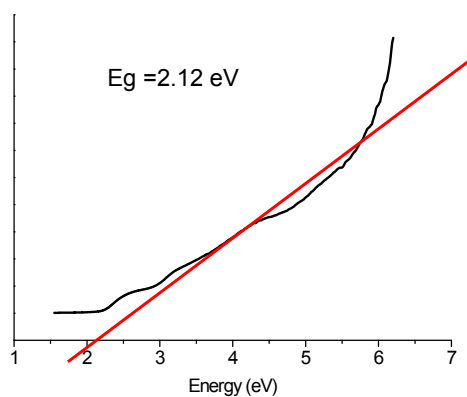Figure S1. The $(Ah\nu)^2$ vs hν curve of **1**.

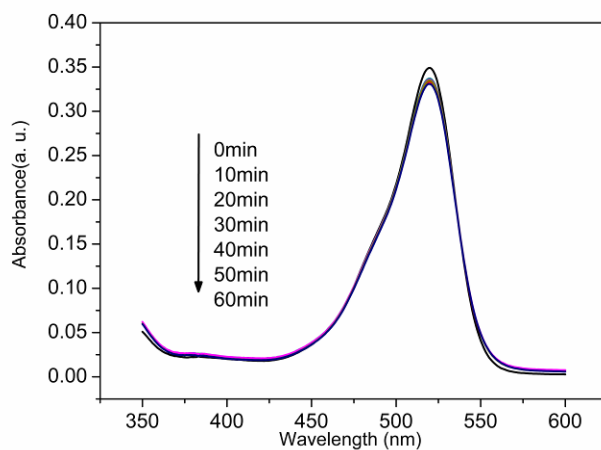Figure S2. The $(Ah\nu)^2$ vs hν curve of **2**.

Figure S3. Concentration changes of R6G on time dependent UV/Vis spectra without photocatalysts in UV light.
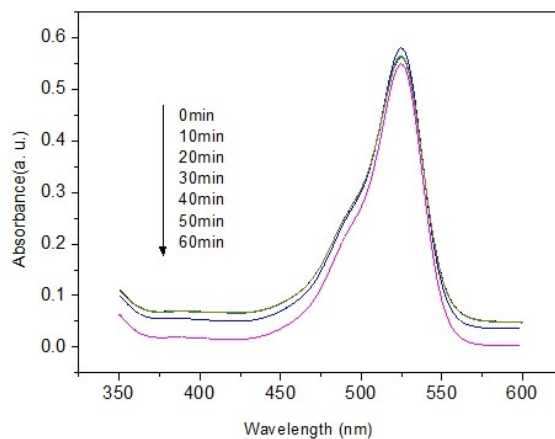

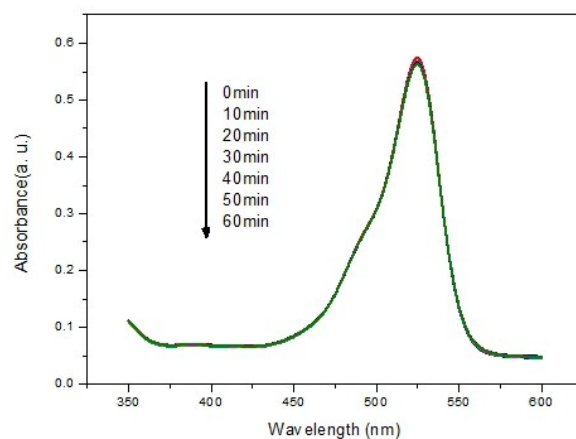Figure S4. Concentration changes of R6G on time dependent UV/Vis spectra with photocatalyst **1** in dark.

Figure S5. Concentration changes of R6G on time dependent UV/Vis spectra with photocatalyst **2** in dark.
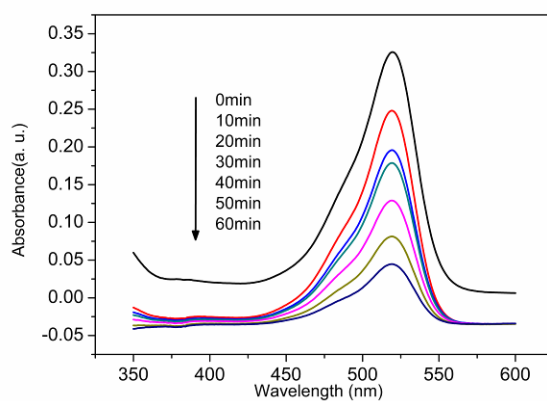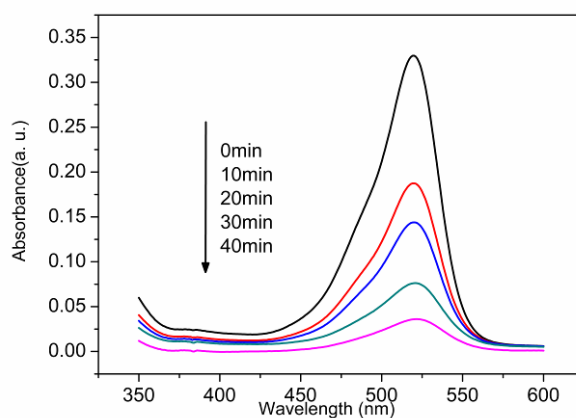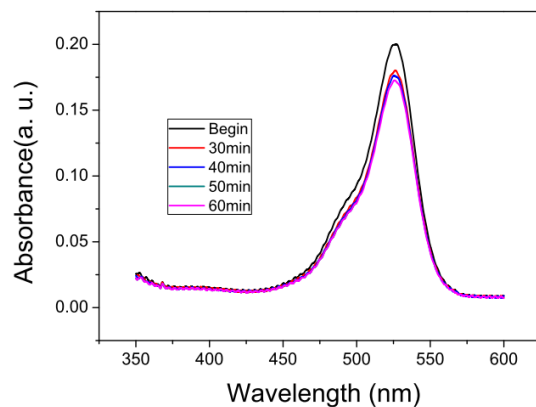

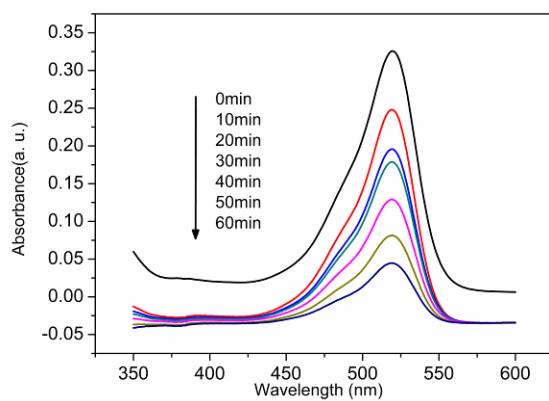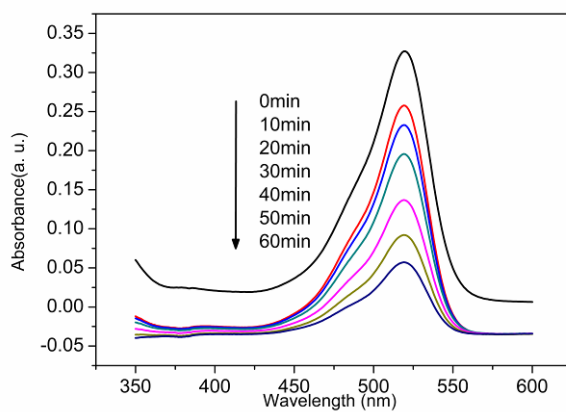Figure S6. Concentration changes of R6G on time dependent UV/Vis spectra with **1** in UV light.

Figure S7 Concentration changes of R6G on time dependent UV/Vis spectra with **2** in UV light.

Figure S8. Concentration changes of R6G on time dependent UV/Vis spectra before and after the photocatalyst **1** filtrated.
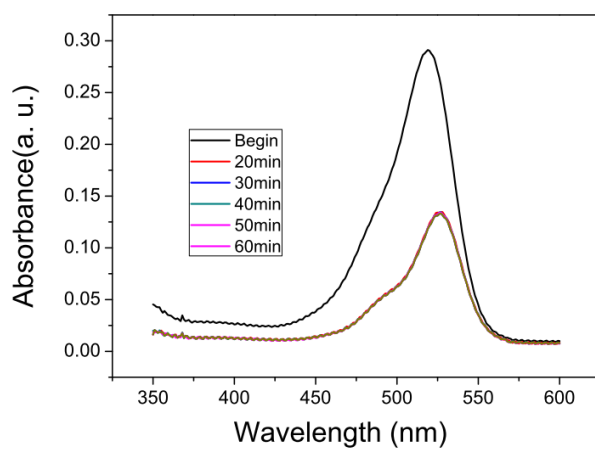
Figure S9. Concentration changes of R6G on time dependent UV/Vis spectra before and after the photocatalyst **2** filtrated.
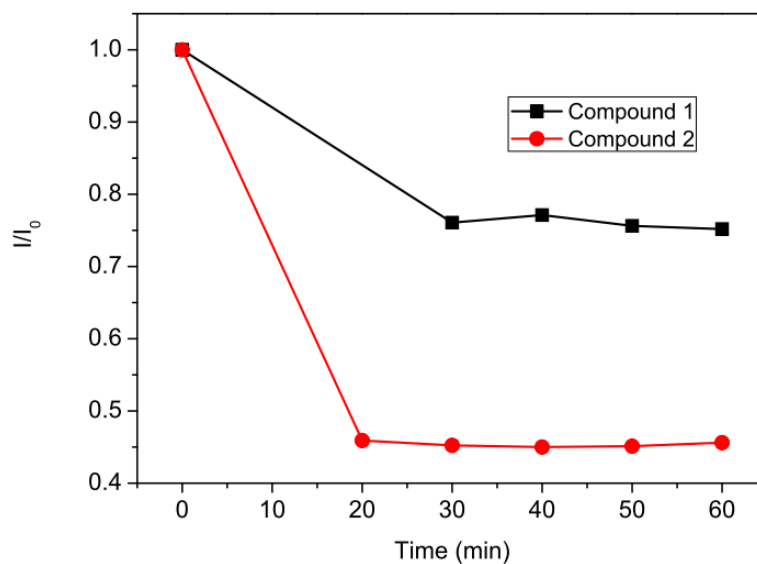
Figure S10. Photodecomposition of R6G in solution with UV light in the condition that the solid catalyst is filtered from the reaction suspensions after 30min of irradiation.

Figure S11. Concentration changes of R6G on time dependent UV/Vis spectra with **1** in the first photocatalytic cycles.
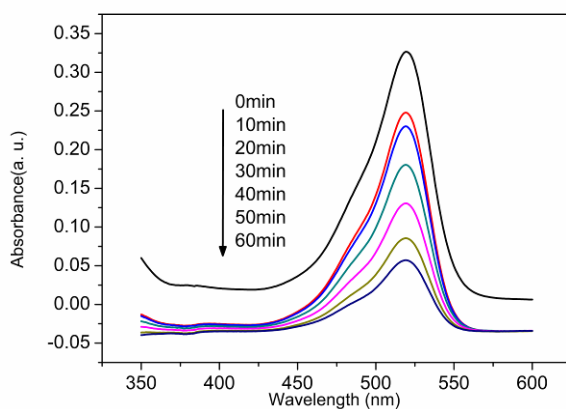
Figure S12. Concentration changes of R6G on time dependent UV/Vis spectra with **1** in the second photocatalytic cycles.

Figure S13. Concentration changes of R6G on time dependent UV/Vis spectra with **1** in the third photocatalytic cycles.
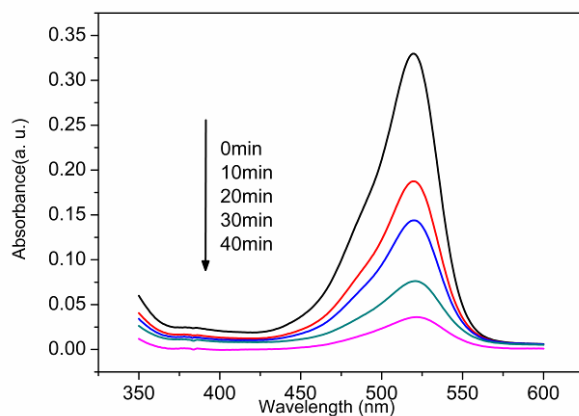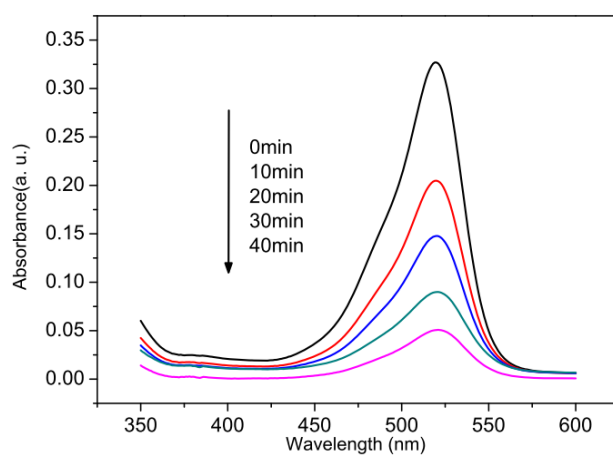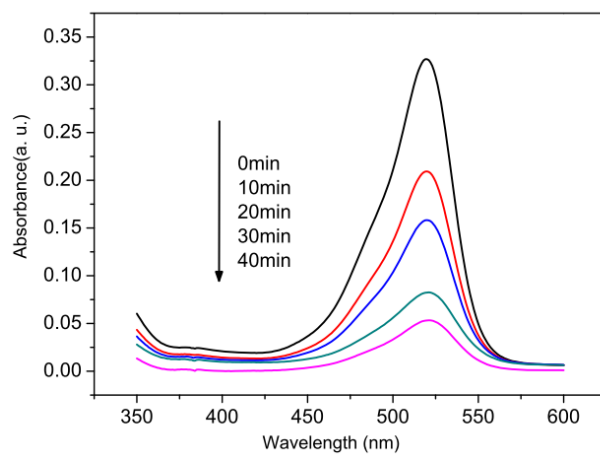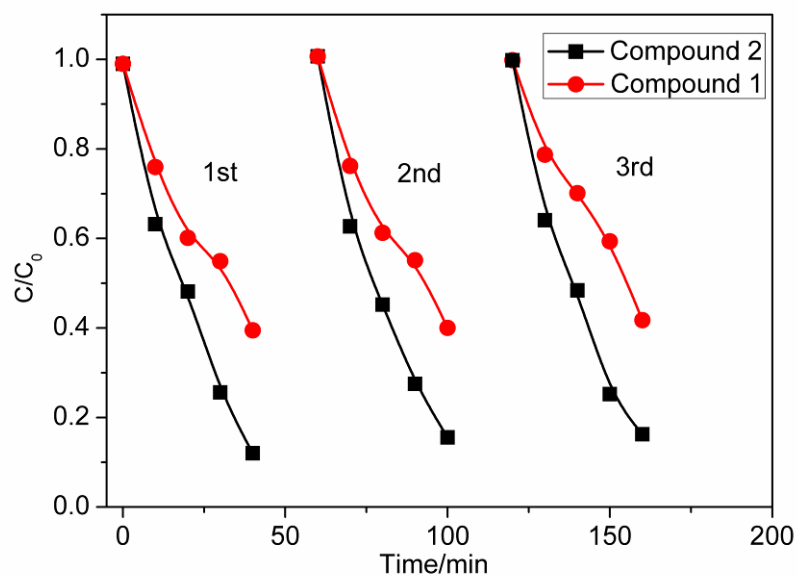
Figure S14. Concentration changes of R6G on time dependent UV/Vis spectra with **2** in the first photocatalytic cycles.

Figure S15. Concentration changes of R6G on time dependent UV/Vis spectra with **2** in the second photocatalytic cycles.

Figure S16. Concentration changes of R6G on time dependent UV/Vis spectra with **2** in the third photocatalytic cycles.

Figure S17. Concentration changes of R6G irradiated with **1** and **2** in three photocatalytic cycles. The results suggested that both **1** and **2** could keep similar photocatalytic efficiencies after three photocatalytic cycles.
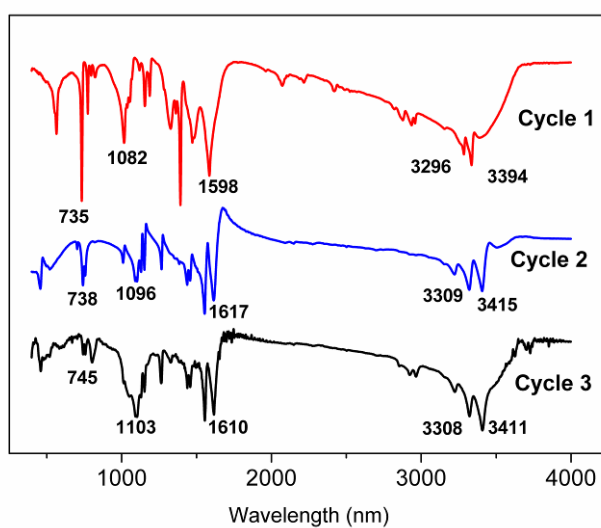

Figure S18. the IR spectra for compound **1** under different photocatalytic cycles.
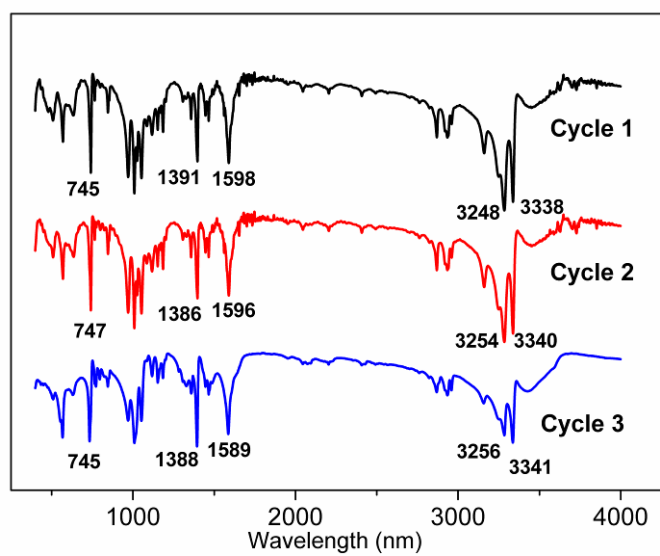
Figure S19. The IR spectra for compound **2** under different photocatalytic cycles.
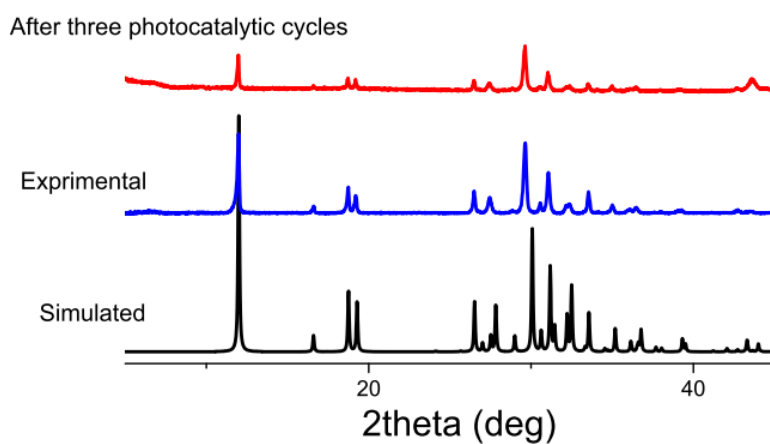

Figure S20. The PXRD patterns of **1** under different conditions. The PXRD traces show diminution in the peaks as the catalyst is reused, and the reason might be due to the lost of crystallinity.
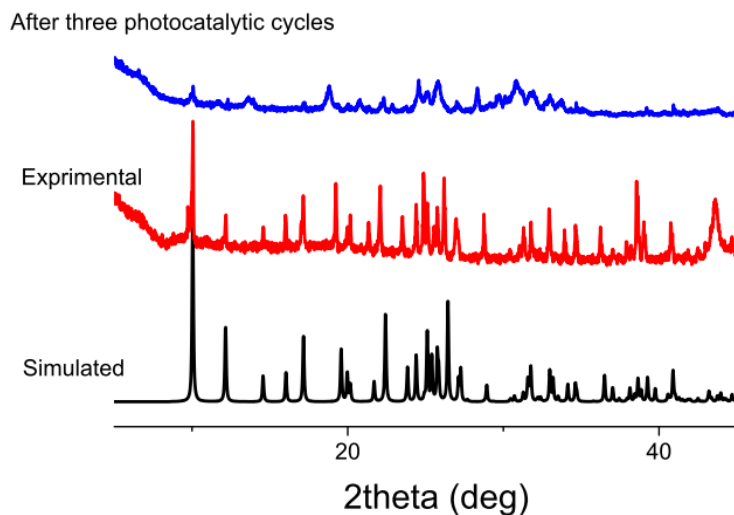
Figure S21. The PXRD patterns of **2** under different conditions. The PXRD traces show diminution in the peaks as the catalyst is reused, and the reason might be due to the lost of crystallinity. And the some obvious peak changes from 35 to 40° after three cycles might be due to the structural distortion or layer shift.
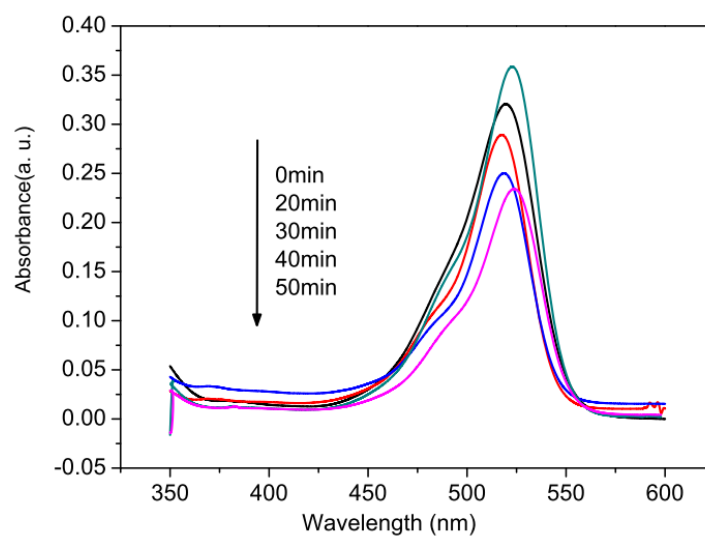

Figure S22. Concentration changes of R6G on time dependent UV/Vis spectra with **2** in visible light.
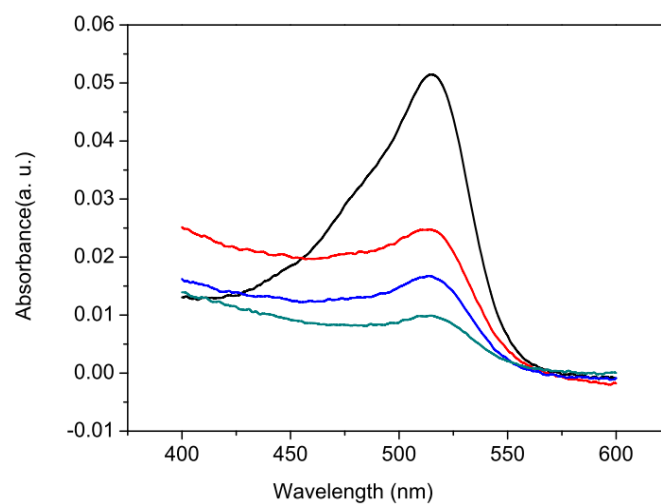
Figure S23. Concentration changes of R6G on time dependent UV/Vis spectra with P-25 in UV light.
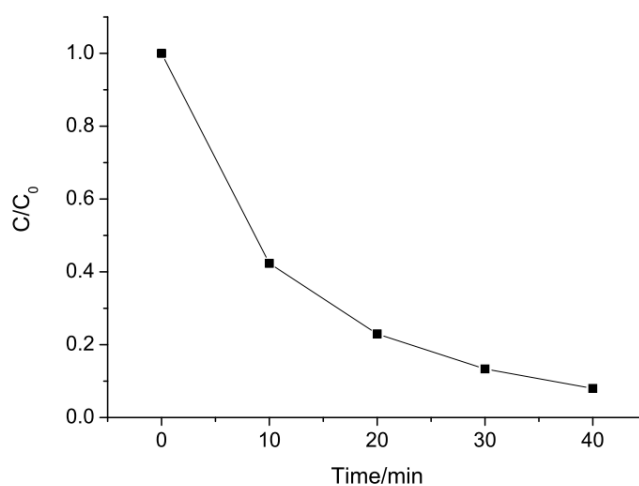

Figure S24. Concentration changes of R6G irradiated with UV light as a function of irradiation time in the present of Degussa P-25.

Table 5. The total organic carbon (TOC) analysis of the organic residues for the photocatalysis experiments of **1** and **2**.

Photocatalyst	Initial consistency of R6G	TOC of degradation products
Compound **1**	4.7901 mg/L	1.3360 mg/L
Compound **2**	4.7901 mg/L	0.9450 mg/L

References:
1 Kisch, H. *Angew. Chem., Int. Ed.*, 2013, **52**, 812.
2 Zhou, L.; W. Z. Wang; S. W. Liu; L. S. Zhang; H. L. Xu and W. Zhu, *J. Mol. Catal. A. Chem.* 2006, **252**, 120.